Chemistry & Biology, Vol. 12, 1317–1324, December, 2005, ©2005 Elsevier Ltd All rights reserved. DOI 10.1016/j.chembiol.2005.09.014

The β-Carboline Analog Mana-Hox Causes Mitotic Aberration by Interacting with DNA

Lan Chun Tu,[1,5] Chien-Shu Chen,[3] I-Ching Hsiao,[2] Ji-Wang Chern,[3] Chi-Hung Lin,[2] Ya-Ching Shen,[4] and Sheau Farn Yeh[1,*]
[1]Institute of Biochemistry and Molecular Biology
School of Life Sciences
[2]Institute of Microbiology & Immunology
National Yang-Ming University
Taipei
Taiwan
[3]School of Pharmacy
College of Medicine
National Taiwan University
Taipei
Taiwan
[4]Institute of Marine Resources
National Sun Yat-sen University
Kaohsiung
Taiwan

Summary

Mana-Hox, an analog of β-carbolines with anticancer activity, induces aberrant mitosis and delays mitotic exit. However, the cellular target is not known. In this study, we visualized the intracellular localization of Mana-Hox. Mana-Hox rapidly penetrated into cells (within 1 min) and concentrated on disorganized metaphase chromosomes after 13 hr of exposure. We demonstrated that Mana-Hox is a noncovalent DNA binder that can interact with DNA through intercalation and/or through minor groove binding. Furthermore, Mana-Hox also inhibits topoisomerase II relaxation activity in vitro, suggesting that Mana-Hox could perturb mitotic chromosome decatenation. Overall, Mana-Hox binding to DNA plays a critical role in the induction of aberrant mitosis and contributes to its anticancer activity.

Introduction

Anticancer drugs interrupt mitosis by targeting the mitotic apparatus or chromosomes [1, 2]. The perturbation of mitotic apparatus by antimicrotubule drugs such as taxol and vinca alkaloids block the cell cycle at mitosis [3]. Unlike antimicrotubule drugs, drugs such as cisplatin and doxorubicin disrupt chromosome integrity and usually block cells' entry into mitosis [4]. However, whether the cell cycle can be blocked before mitosis following DNA damage may depend on whether cells can detect changes or damages on chromosome DNA [5–7].

Whether DNA damaging or binding agents induce significant changes on DNA can depend on their interaction with DNA. DNA binding agents can bind to DNA by either covalent or noncovalent interaction [8]. Covalent binding agents such as cisplatin directly induce lesions on the DNA template, while noncovalent binding agents such as ethidium bromide and benzimidazole do not. It is known that noncovalent interactions rely on the strength of electrostatic interactions, i.e., hydrogen bonding and van der Waals interactions. Such interactions cannot produce stable drug-DNA complexes [8, 9], and they, therefore, do not significantly damage DNA unless DNA enzymes such as topoisomerase intervene [9]. Noncovalent DNA binding can alter chromatin structure by unwinding the DNA helix or widening the minor groove [10–12]. Since endogenous DNA binding proteins such as TBP also alter DNA structure [13, 14], it is not known if cells would be aware of similar changes induced by a noncovalent DNA binding agent.

Noncovalent DNA binding agents often possess structural characteristics such as planar aromatic ring systems and basic side chains [8, 9]. Many natural products and their derivatives, such as anthracyclines, pyridocarbazoles, and β-carboline alkaloids, also possess such structural characteristics and can intercalate or bind to the DNA minor groove [15, 16]. Our previous study identified a synthetic analog of β-carboline Mana-Hox [17] **1** (Figure 1). It is composed of a β-carboline and a carbazole chromophore and exhibits anticancer activity on several human cancer cell lines [18]. **1** induces cancer cell death by interfering with mitosis. After cells are treated with **1**, many aberrant mitotic cells, including those with bipolar spindles and lagged chromosomes and those with multipolar spindles and disorganized chromosomes, appear and are accompanied by the activation of the spindle checkpoint that delayed cell exit from mitosis. The aberrant mitotic cells eventually exit mitosis, resulting in chromosome missegregation and cell death. However, **1** is not an antimicrotubule agent. The impairment of mitosis by **1** does not result from the inhibition of microtubules.

In this study, we examined the DNA binding activity of **1** in intact cells and in a cell-free system. We demonstrated that **1** both binds and intercalates in the DNA minor groove. The binding of **1** to chromosomal DNA plays a critical role in its induction of aberrant mitosis.

Results

Mana-Hox Binds to Nuclear DNA

1 exhibits absorption in both the near-UV region and the visible region. Two absorption bands, centered at 287 nm and 350 nm, are known to be associated with the carboline moiety. Another absorption band, centered at 414 nm, is caused by the carbazole moiety (data not shown). We took advantage of its absorption property to visualize the localization of **1** in live cells. HeLa cells were treated with 4 μM **1** and observed directly by a fluorescence microscope under UV excitation. As shown in Figure 2A, fluorescent signals of **1** were detected inside the cell after 1 min of drug exposure as punctuate spots that gradually concentrated around the nuclear envelope (10 min and 60 min). After 5 hr, the fluorescence of **1** was

*Correspondence: fyeh@ym.edu.tw
[5]Present address: The Institute for Systems Biology, Seattle, Washington 98103.

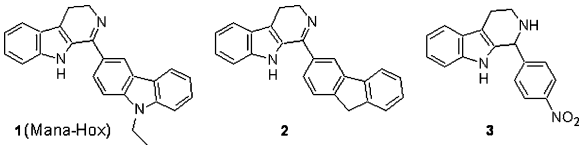

Figure 1. Structure of Mana-Hox and Analogs

found in the nucleus (double arrows) and the nucleolus (double arrowheads).

The fluorescent signals of **1** progressively accumulated in the area next to the nucleus that corresponded to the Golgi apparatus (Figure 2A, arrows), endoplasmic reticulum (ER), and mitochondria (Figure 2A, arrowheads, 60 min panel). To test if **1** distributes in these subcellular compartments, HeLa cells were transfected with probes specific for the Golgi, ER, and mitochondria as described in Experimental Procedures. Cells were treated with **1** at 12 hr posttransfection. As shown in Figure 2B, **1** accumulated mainly in the Golgi complexes (arrows) at 1 min of exposure. After 60 min, **1** appeared in the reticulum or rod-shaped organelles (arrowheads), including ER (Figure 2C) and mitochondria (Figure 2D).

1 is known to induce aberrant mitosis [18]. To determine whether **1** binds to abnormal metaphase chromosomes, HeLa cells were treated with **1** for 13 hr and observed by fluorescence microscope. As shown in Figure 2E, the fluorescence of **1** appeared in lagged chromosomes (a and b, arrows), Y-shaped chromosomes (c, dashed line), and other disorganized chromosomes (d). Cells that were then stained with the DNA dye Hoechst 33258 further demonstrated that **1** colocalized with chromosome DNA (Figure 2F).

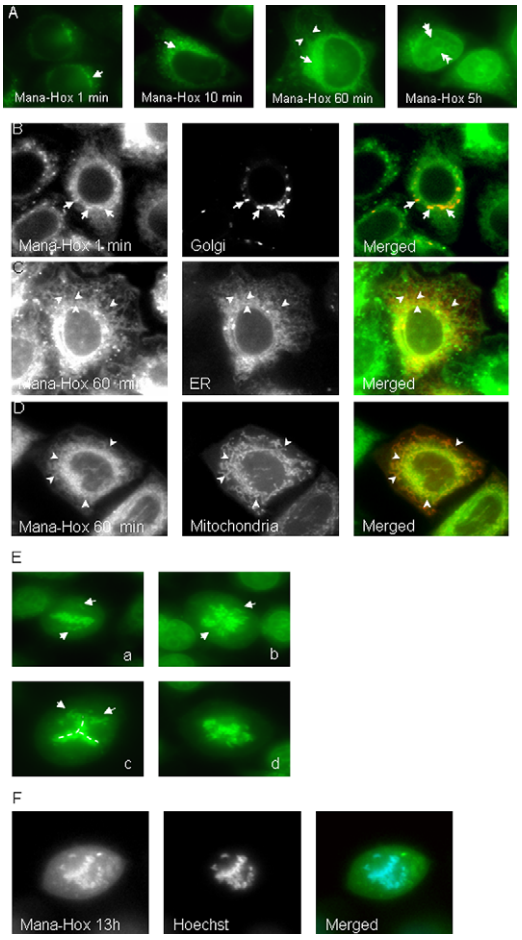

Figure 2. Cellular Localization of Mana-Hox in HeLa Cells

(A) HeLa cells were exposed to 4 μM **1** for 1 min, 10 min, 60 min, or 5 hr. After drug removal, cells were observed with a fluorescence microscope, and the presence and distribution of **1** were determined by its fluorescence.

(B–D) HeLa cells were transfected with organelle markers as described in Experimental Procedures. Cells were treated with **1** for the indicated time at 12 hr posttransfection. The colocalization of **1** and the subcellular organelles were examined with a fluorescence microscopy.

(E) HeLa cells were exposed to 4 μM Mana-Hox for 13 hr. After drug removal, cells were observed with a fluorescence microscope. Note the accumulation of **1** in the aberrant metaphase chromosomes.

(F) Drug treatments were as described in (E). The presence of Mana-Hox (stained green) in the aberrant metaphase chromosomes was confirmed by the staining with the DNA dye Hoechst 33258 (stained blue).

Mana-Hox Directly Binds to DNA

To test if **1** directly binds to DNA, fluorescence emission spectra were measured with an excitation wavelength of 287 nm. The binding of **1** to DNA was characterized by a decrease of the fluorescence intensity (hypochromicity) between 350 and 375 nm until a DNA/drug (P/D) ratio of 2.5 was reached (Figure 3). In contrast, fluorescence intensity was increased (hyperchromicity) between 495 and 520 nm with a wavelength shift of about 5–20 nm depending on DNA concentration, indicating that the binding of DNA altered the geometry of **1**. Similar results were also obtained when the excitation wavelength was set at 350 and 414 nm (data not shown). Scatchard plots were made based on the fluorescence data obtained at 372 and 520 nm and were fitted into a two-site model [19]. This resulted in the determination of two binding sites, $n_1 = 1.5 \pm 0.06$ and $n_2 = 2.7 \pm 0.01$, with two binding constants, $K_1 = 6.5 \pm 0.3 \times 10^6\ M^{-1}$ and $K_2 = 1.6 \pm 0.1 \times 10^6\ M^{-1}$, respectively. These fluorescence measurements indicate that **1** binds to DNA.

Mana-Hox Quenches the Fluorescence of Ethidium Bromide-DNA Complexes

Hypochromicity is known to be associated with many DNA intercalators [20, 21]. To test if **1** would intercalate DNA, we utilized the ethidium bromide displacement assay, in which another intercalating agent would reduce the fluorescence intensity caused by ethidium bromide-DNA complexes. Calf thymus DNA was incubated with ethidium bromide and **1** in various proportions. The alteration of fluorescence was measured with a fluorometer. As shown in Figure 4A, the addition of **1** reduced the fluorescence of ethidium bromide-DNA in a concentration-dependent manner. The C_{50} value was 10 μM. By contrast, the other analogs, **2** and **3**, showed no effect on the fluorescence intensity of ethidium bromide-DNA.

Mana-Hox Causes Mobility Retardation of Supercoiled DNA

To further examine the interaction between **1** and DNA, we observed the mobility of supercoiled DNA on agarose gels in the presence or absence of **1**. As shown in

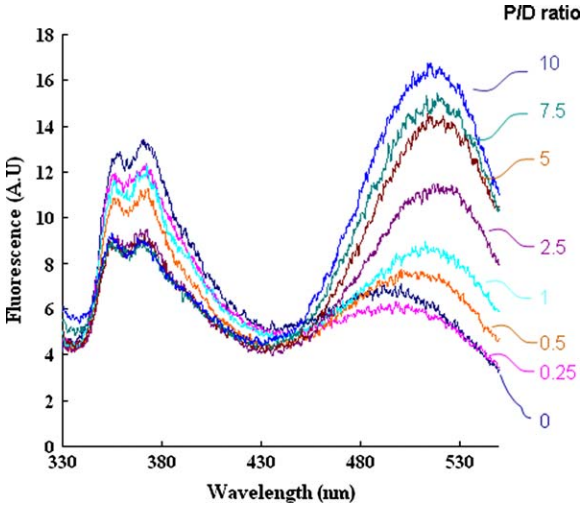

Figure 3. Fluorescence Spectrum of Mana-Hox and Its Alteration upon the Addition of DNA

Solutions were excited at 287 nm, and emission spectra were recorded. Solutions consist of 1 μM **1** (D) and calf thymus DNA (P) at 0.25, 0.5, 1, 2.5, 5, 7.5, and 10 μM.

Figure 4B, the mobility of the supercoiled plasmid DNA was retarded in the presence of **1** in a concentration-dependent manner (lane 1 and lanes 3–9). At a concentration of 50 μM and above, the **1**-induced mobility shift reached a plateau. Ethidium bromide (lane 2) is known to relax superhelical DNA and induce a significant mobility shift. Another drug, taxol, which is not known to bind to DNA, did not induce a plasmid DNA mobility shift, and it served as a negative control (lane 10). Similar results were obtained when this experiment was performed with a linear DNA marker (data not shown; Figure S1).

Mana-Hox Quenches the Fluorescence of Hoechst-DNA Complexes

Hyperchromicity is a characteristic of many DNA minor groove binders. To test if **1** is a DNA minor groove binder, a competition titration with Hoechst 33258 was performed. Calf thymus DNA was incubated with Hoechst 33258 and **1** in various proportions. The alteration of fluorescence was measured with a fluorometer. As shown in Figure 4C, the addition of **1** reduced the fluorescence intensity of Hoechst-DNA in a concentration-dependent manner. The C_{50} value was 2.5 μM. By contrast, the other analogs, **2** and **3**, showed no effect on the fluorescence intensity.

Mana-Hox Can Bind to DNA through Intercalation and the Minor Groove

To predict a possible binding mode of **1** and DNA, a docking study was conducted by using the AutoDock program [22, 23]. The reference DNA double helix coordinate used for docking was a B form duplex DNA, 5′-d(CCGGCGGT)-3′. As shown in Figure 5A, the indolyl moiety of the carboline skeleton intercalated between GC base pairs and formed hydrogen bonds via a water-mediated interaction (Figure 5A, c), and it placed the carbazole moiety in the minor groove. The docking energy was −12.36 kcal/mol (Table 1). Analog **2** does not have

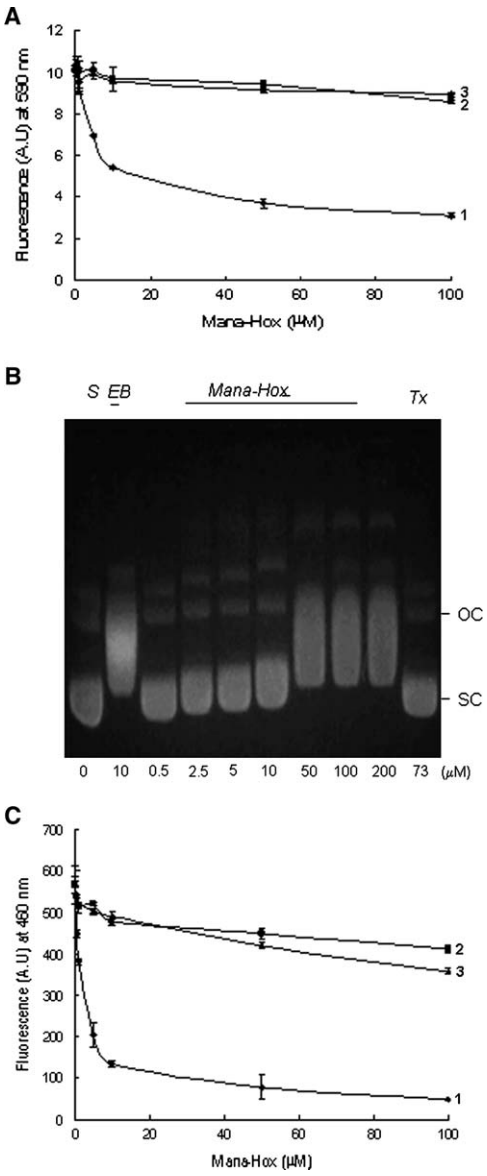

Figure 4. Mana-Hox Can Intercalate DNA and Bind to the DNA Minor Groove

(A) Quenching of fluorescence intensity of the ethidium bromide-DNA complex by Mana-Hox and analogs. Calf thymus DNA (20 μM) was preincubated with 2 μM ethidium bromide in 0.01 M ionic strength buffer, and was then incubated separately with **1**, **2**, and **3** in various concentrations for another 10 min. The samples were excited at 538 nm, and the fluorescence was measured at 590 nm (mean ± SEM; n = 3).

(B) Effect of Mana-Hox on the electrophoretic mobility of supercoiled DNA. pC86 (2 μg) was preincubated with various concentrations of **1** for 30 min, loading buffer was then added, and the samples were electrophoresed through 1% agarose gels. Abbreviations: S, plasmid DNA; EB, ethidium bromide; Tx, taxol; OC, nicked, open circular DNA; SC, supercoiled DNA.

(C) Quenching of fluorescence intensity of the Hoechst 33258-DNA complex by Mana-Hox and analogs. Calf thymus DNA (1 μg) was preincubated with 6.1 μM Hoechst 33258 in PBS for 10 min at room temperature, and was then incubated separately with **1**, **2**, and **3** in various concentrations for another 10 min. The samples were excited at 355 nm, and the fluorescence was measured at 460 nm (mean ± SEM; n = 3).

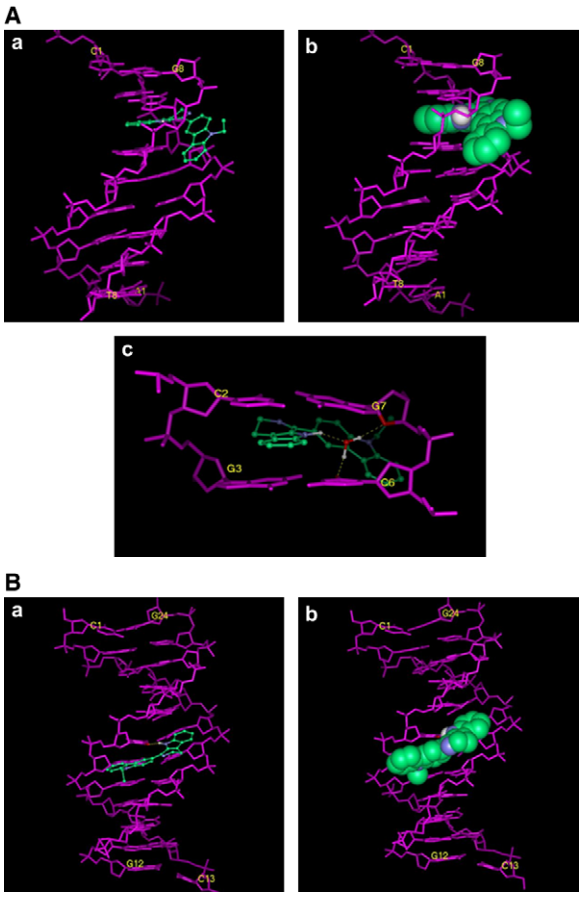

Figure 5. The Energy-Minimized Docked Model of the Mana-Hox-DNA Complex

(A) The lowest-energy docked conformations proposed the energetically favorable binding of **1**, with the β-carboline moiety being intercalated into d(CCGGCGGT)$_2$. a, line plot; b, space-filling plot. c, hydrogen bonding interactions in the intercalation site of the energy-minimized docked model of the **1**-DNA complex. The water molecule was from the solvation calculations.

(B) The lowest-energy docked conformations proposed the energetically favorable binding of **1** to d(CGCAAATTTGCG)$_2$ through the minor groove. a, line plot; b, space-filling plot. The following color scheme is used: **1**: carbon, green; nitrogen, blue; hydrogen, white; hydrogen bond, white dotted line; oxygen, red; DNA duplex, purple.

an N-ethyl group on the carbazole moiety, and it experienced a gain in docking energy of 0.6 kcal/mol (−11.76 versus −12.36 kcal/mol) (Table 1 and Figure S2A). In analog **3**, a nitrophenyl group replaces the carbazole moiety and exists in *R* and *S* configurations. These two stereoisomers were docked separately into the intercalation site. The lowest docking energy was −6.33 and −5.39 kcal/mol for *R* and *S* isomers (Table 1 and Figure S2A), respectively.

1 was also docked into another reference DNA double helix, a DNA dodecamer, d(CGCAAATTTCGCG)$_2$, in complex with the minor groove binder Hoechst 33258 (PDB code: 264d). The suggested minor groove binding mode is shown in Figure 5B. **1** adopts a conformation with a dihedral angle of 31° between the β-carboline and carbazole rings, enabling it to fit well in the minor groove. The β-carboline NH of **1** is hydrogen bonded to the O-2 atom of thymidine designated T19. The N-ethyl group of **1** is deeply inserted into the groove to where it interacts with DNA via van der Waals forces. The docking energy was −12.6 kcal/mol (Table 1).

Table 1. Docking Energies of Compounds **1**–**3** Docked into DNA with the AutoDock 3.0 Program

Compound	Docking Site	Docking Energy (kcal/mol)[a]
1 (Mana-Hox)	Intercalation cavity	−12.36
2	Intercalation cavity	−11.76
3 (*R* isomer)	Intercalation cavity	−6.33
3 (*S* isomer)	Intercalation cavity	−5.39
1 (Mana-Hox)	Minor groove	−12.60
2 (Model I)	Minor groove	−11.33
2 (Model II)	Minor groove	−10.93
3 (*R* isomer)	Minor groove	−6.49
3 (*S* isomer)	Minor groove	−7.68
1 (Mana-Hox)	Major groove	−8.98

The energy calculations were performed by using the AutoDock 3.0 energy scoring function.

[a] The value is the lowest docking energy for each compound, with the exception of **2** (Model II).

In comparison with **1**, the lowest docking energy of **2** was determined to be −11.33 kcal/mol (Table 1, Model I of **2**; Figure S3B), indicating that no intermolecular hydrogen bond is formed by the NH group of **2**. When **2** adopts a docking orientation similar to that of **1**, the resulting docking energy of the **2**-DNA complex (Model II of **2**) is less stable by 1.67 kcal/mol (−10.93 versus −12.6 kcal/mol) due to the lack of the N-ethyl group. Analogs **3***R* and **3***S* were docked differently into the minor groove. The lowest docking energy was −6.49 and −7.68 kcal/mol for the *R* and *S* isomers (Table 1 and Figure S3C), respectively.

Mana-Hox Inhibits Topoisomerase II Relaxation Activity

It is known that many minor groove binders can also inhibit topoisomerase activity [24, 25]. The effect of **1** on topoisomerase II (topo II) activity was determined by measuring the relaxation of plasmid DNA. Supercoiled plasmid DNA (Figure 6, lane 1) was completely relaxed in the presence of topo II (lane 2) and partially relaxed in the presence of etoposide (lane 3), which is a known topo II inhibitor. **1** at concentrations less than 50 μM did not inhibit topo II relaxation of supercoiled DNA (lanes 6–9), but, at 50 and 100 μM, the relaxation was substantially inhibited (lanes 4 and 5). The mobility shift of supercoiled DNA in the presence of 50 and 100 μM **1** might also result from DNA intercalation (lanes 4 and 5).

Discussion

Induction of aberrant mitosis has been found in many antimicrotubule agent-treated cells. Since antimicrotubule agents can modify microtubule behavior and impair spindle fiber formation, the subsequent activation of spindle assembly checkpoints prevents cell exit from mitosis, causing the appearance of abnormal mitotic cells such as monopolar and multipolar mitotic cells, and resulting in chromosome missegregation. Our previous study found a novel anticancer agent **1**, which also delays cell exit from mitosis and causes aberrant

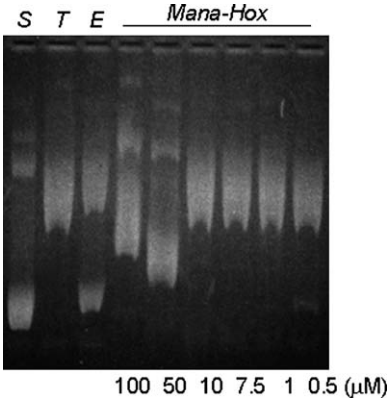

Figure 6. Mana-Hox Inhibits Topoisomerase II Relaxation

Plasmid DNA (1 μg) was incubated with various concentrations of **1**, and was then treated with 8 U topoisomerase II for 30 min at 37°C. The reaction was stopped by adding EDTA/SDS. The samples were electrophoresed through 1% agarose gel. S, supercoiled DNA; T, topoisomerase II; E, etoposide (85 μM).

mitosis yet is not an antimicrotubule agent [18]. In this study, we demonstrated that **1**-induced aberrant mitosis is a result of noncovalent DNA binding.

Based on live cell images, **1** rapidly penetrated the cell membrane and distributed to membranous organelles, but it was not detectable in interphase nuclei until 5 hr posttreatment (Figure 2). **1** was minimally detectable in interphase nuclei (Figure 2A, 5 hr), possibly because a large percentage of **1** was retained in the membranous organelles and/or the fluorescence was easily quenched on noncondensed chromosomes. When **1** induced significant numbers of cells to arrest in metaphase (13 hr), the fluorescence of **1** appeared on the mispositioned chromosomes and colocalized with Hoechst staining (Figures 2E and 2F), indicating that **1** is in contact with DNA. Our other study with fluorescence lifetime measurements (Shiao and C.-H.L., unpublished data) also supports the idea that **1** binds to nuclear DNA. These results raised the question as to how a DNA binding agent can induce mitosis arrest without slowing down S phase progression. In general, drugs that bind to DNA can introduce lesions on the DNA template and block DNA replication. In response to DNA binding/damaging agents, cells can activate DNA damage checkpoints to prevent entry into mitosis with damaged DNA or incompletely replicated DNA [26]. However, **1** does not impede cell cycle progression through S phase [18], suggesting that the binding of **1** to DNA might not induce DNA damage. The binding of **1** to DNA apparently influences the alignment of chromosomes on spindle fibers, indicating that **1** might alter DNA structure and interfere with DNA binding proteins that are required for chromosome segregation [27].

The influences of **1** on DNA can be explained by its interaction with DNA in vitro. The addition of DNA to **1** caused two significant alterations to the fluorescence emission spectrum. The hypochromicity effect (Figure 3) is also found to be associated with several classical DNA intercalators such as ethidium bromide, cryptolepine, matadine, and acridine [20, 21], suggesting that **1** exhibits its DNA intercalation activity. Consistent with this observation, **1** displaced ethidium bromide from DNA, resulting in the decrease of the fluorescence of ethidium bromide-DNA complexes (Figure 4A). The binding constant K_a calculated from this assay was $2.44 \times 10^6\ M^{-1}$, which is close to the K_2 calculated from a fluorescence emission spectrum. In addition, **1** also retarded linear marker DNA (data not shown and Figure S1) and supercoiled plamid DNA migration during agarose gel electrophorsis (Figure 4B), further demonstrating that **1** can intercalate with DNA.

The hyperchromicity and red shift effect (Figure 3) have been found in DNA minor groove binders such as Hoechst 33258 [10], suggesting that **1** can also bind to DNA through minor groove interaction. In agreement with this observation, **1** quenched the fluorescence induced by Hoechst-DNA complexes (Figure 4C). The K_a value was $5.8 \times 10^6\ M^{-1}$, which is close to the K_1 value calculated from a fluorescence emission spectrum. Of note, the C_{50} values of **1** in the reduction of Hoechst-DNA complex fluorescence was 4-fold lower than that for ethidium bromide-DNA complexes (Figures 4A and 4C). It is also known that the C_{50} value of an intercalator in the ethidium bromide displacement assay is usually higher than 20 μM. The C_{50} value of **1** is less than 15 μM, indicating that it preferentially binds to DNA through interaction with the minor groove [28, 29]. Furthermore, based on chemical structure, **1** contains a 3,4-dihydropyridoindole (dihydro β-carboline) and an N-ethylcarbazole [17]. Chemicals containing one of these chromophores are known DNA intercalators [9]. However, unlike other simple β-carboline alkaloids such as harman and norharman [30], our results revealed that **1** can intercalate DNA and also bind to the DNA minor groove.

When **1** was docked into a GC-rich B form of DNA, only the indole part of the β-carboline moiety inserted into the GC base pairs, unlike simple β-carboline alkaloids or carbazole derivatives of which the planar chromophore intercalates between nitrogen base pairs. It is known that the planar aromatic ring systems stack with the DNA base pairs, and that this interaction is important for DNA intercalation. However, **1** is a dihydro β-carboline in which the conformation of dihydro pyridine hampers the planar surface and impedes **1** stacking with DNA base pairs with its entire β-carboline moiety (Figure 5A). Since there is only one single bond distance between the dihydro β-carboline and the carbazole moiety, **1** cannot intercalate DNA like a bis-intercalator. Rather, the angle between the dihydro β-carboline and the carbazole moiety results in the carbazole moiety hanging over the DNA minor groove. This result supports the indication that **1** may be a nonclassical DNA intercalator, which partially stacks with DNA base pairs [16, 31] and partially occupies the DNA minor groove.

Like many DNA minor groove binders, **1** is composed of two heteroaromatic rings linked together directly through a single bond [16, 32]. When **1** was docked into the DNA minor groove, **1** adopted a conformation similar to that of Hoechst 33258 and formed a stable complex in the DNA minor groove. However, **1** can only bind to an AT-rich, but not GC-rich, DNA minor groove (Figure 5B). It is possible that the electron density of an AT-rich DNA minor groove is more compatible with **1**. This prediction was also consistent with our finding that the addition of poly (AT) to **1** caused hyperchromicity at longer

wavelengths, but loss of the hypochromicity effect at short wavelengths (data not shown). Therefore, whether **1** binds to DNA like a nonclassical DNA intercalator or like a DNA minor groove binder may be influenced by the sequence of the DNA binding motif. On the other hand, since **1** is such a small molecule, it is also possible that it fits into the DNA major groove. We therefore performed another docking experiment that showed that the resulting **1**-DNA complex in the major groove was less stable than that in the minor groove. The docking energy was higher than that of the minor groove binding and intercalation (Table 1).

Compared to **1**, analogs **2** and **3** (Figure 1) did not exhibit any DNA binding activities in our experiments (Figure 4 and data not shown). Molecular simulation studies revealed that neither **2** nor **3** are able to form an energetically favorable DNA complex, suggesting that the **1**-substitution on 3,4-dihydro β-carboline and the N-alkyl side chain on carbazole is important for stable DNA binding.

DNA intercalators and minor groove binders such as simple β-carboline alkaloids, quinacrine, benzimidazole, and distamycin are known to inhibit DNA topoisomerase activity [24, 33–35]. **1** also inhibited topo II-mediated DNA relaxation in vitro. Topo II is a known key enzyme involved in DNA decatenation, which has to be completed before cells exit from mitosis. Interference with the function of topo II, such as that seen with topo II inhibitor ICRF-193, can delay cell exit from mitosis and cause chromosome missegregation [36, 37]. However, the concentration that is required for **1** to inhibit topo II was above 50 μM; whether **1**-induced aberrant mitosis relates to the inhibition of topo II requires further studies. Moreover, **1** does not inhibit topo I (data not shown), indicating that **1** does not inhibit DNA replication.

Our study demonstrates that **1** is a noncovalent DNA binder that intercalates and binds DNA in the minor groove. The binding of **1** to chromosome DNA does not inhibit S phase progression [18], indicating that DNA binding alone is not sufficient to inhibit DNA replication or induce DNA damage (responses). Indeed, we did not observe any activation of DNA damage stress responses such as those involving p53, p38, and MAPK after treatment with **1** (data not shown). However, noncovalent DNA binding can alter the topology of DNA [12]. It is possible that the alteration of DNA structure after binding of **1** to DNA affects chromosome alignment and segregation in mitosis. Elucidation of the mechanisms by which **1** alter DNA structure requires further study.

Significance

β-Carbolines are known noncovalent DNA binders, but the biological effects of this binding are not well understood. Herein, we identified DNA as a molecular target by which Mana-Hox induces aberrant mitosis. To our knowledge, Mana-Hox is the first DNA binder that does not impede the function of DNA, but impairs chromosome segregation in mitosis. Since Mana-Hox exhibits anticancer activity, but is not toxic to normal cells, the molecular mechanisms by which Mana-Hox executes its anticancer activity could provide a model for future development of β-carboline analogs as anticancer agents.

Experimental Procedures

Reagents and Cell Culture

Compounds **1**, **2**, and **3** were dissolved in absolute ethanol (Merck). Paclitaxel and Hoechst 33258 were obtained from Sigma Chemical Co. (St. Louis, MO, USA) and were dissolved in absolute ethanol and distilled water, respectively. Etoposide was purchased from Calbiochem Co. (San Diego, CA, USA) and was dissolved in absolute ethanol. Calf thymus DNA and topoisomerase II were purchased from GE healthcare. Streptomycin, penicillin, fetal bovine serum, L-glutamine, nonessential amino acids, and DMEM were obtained from Invitrogen (Grand Island, NY, USA).

HeLa cells were obtained from American Type Culture Collection (ATCC) and were cultured in Dulbecco's modified Eagle's medium (DMEM) medium supplemented with 10% fetal bovine serum, 100 U/ml penicillin, 100 μg/ml streptomycin, 100 μg/ml L-glutamine, and 100 μg/ml nonessential amino acids.

Intracellular Mana-Hox Localization

HeLa cells were seeded on a coverslip, which was precoated with fetal bovine serum for 30 min prior to cell seeding. Cells were treated with 4 μM **1** for the indicated time, the coverslip was washed with PBS, and the cells were observed with a fluorescence microscope (IX71, Olympus, Tokyo, Japan) under UV excitation (λ = 365 nm generated by mercury arc). For the colocalization studies, HeLa cells were transfected with pEYFP-Golgi, pEYFP-ER, or pEYFP-Mitochondria vectors (Clontech) according to the standard protocols (GeneJuice, by Novagen). A total of 12 hr posttransfection, cells were treated with 4 μM Mana-Hox for the indicated time and were observed with fluorescence microscopy.

Fluorescence Emission Spectrum Measurement

1 at 1 μM was incubated with various concentrations of calf thymus DNA in 0.01 M ionic strength STE buffer (9.4 mM NaCl, 2 mM Tris-HCl [pH 7.0], 20 μM EDTA) [38]. Drug solutions with or without calf thymus DNA were excited at 287, 350, or 414 nm, and emission spectra were recorded with a F4500 spectrophotometer (Hitachi, Japan).

DNA Dye Displacement Assays

For ethidium bromide displacement [39], 20 μM calf thymus DNA was preincubated with 2 μM ethidium bromide in 0.01 M ionic strength STE buffer, and was then incubated with **1**, **2**, and **3** in various concentrations for another 10 min. The samples were excited at 538 nm, and the fluorescence was measured at 590 nm with a fluorometer (Fluoroskan Ascent, Labsystems, Japan). For the Hoechst displacement assay [40], 1 μg calf thymus DNA was preincubated with 6.1 μM Hoechst 33258 in PBS for 10 min at room temperature, and was then incubated with **1**, **2**, and **3** in various concentrations for another 10 min. The samples were excited at 355 nm, and the fluorescence was measured at 460 nm. C_{50} is the concentration of DNA binding agent needed to reduce the fluorescence of dye DNA by 50%. The fluorescence of **1** alone is undetectable in both cases.

Gel Mobility Shift Assay

Supercoiled plasmid pC86 [41] or a 1 kb DNA ladder (2 μg) was preincubated with 10 μM ethidium bromide or various concentrations of **1** for 30 min at room temperature, followed by the addition of 1/6 volume 6× loading buffer (0.25% bromophenol blue, 0.25% xylene cyanol, 50% glycerol) and electrophoresis through a 1.5% agarose gel at 90 V for 2 hr in 0.5× Tris-borate-EDTA buffer at room temperature [42]. Next, the gels were stained with ethidium bromide, destained, and then photographed under UV illumination.

Molecular Modeling

The 3D structures of **1**, **2**, and **3** were generated by using SYBYL 7.0 (Tripos Associates; St. Louis, MO, USA) and were optimized with the Tripos force field. The partial atomic charges were calculated by using the Gasteiger-Marsili method. The flexible torsions for **1** were defined with AutoTors implemented in the AutoDock 3.0 software package (The Scripps Research Institute; La Jolla, CA) [22, 23]. In regard to intercalation modeling, a B form duplex DNA model with the sequence 5′-d(CCGGCGGT)-3′ was built by using the BIOPOLYMER/BUILD module in SYBYL. Hydrogen atoms were added, and Kollman All-Atom charges were assigned to the DNA molecule. For the

generation of an intercalation cavity, **1** was manually docked into DNA, where the carboline ring was positioned between two base pairs (CC | GGCGGT), while the carbazole ring was located in the minor groove. This initial complex structure was then optimized by energy minimization with the Tripos force field, employing the Powell method with an energy-gradient-convergence criterion of 0.05 kcal/(mol·Å) and a distance-dependent dielectric constant of 4r. **1** and nonpolar hydrogens were removed from the energy-minimized complex, and the residual DNA was assigned with Kollman United-Atom charges. The resulting DNA structure with an intercalation cavity was used in the docking study of **1** with the AutoDock program.

To carry out AutoDock simulations, a grid box was defined to enclose the intercalation cavity with dimensions of 18.8 × 18.8 × 18.8 Å and a grid spacing of 0.375 Å. The grid maps for energy scoring were calculated by using AutoGrid. Docking was performed by using the Lamarckian genetic algorithm (LGA) and the pseudo-Solis and Wets local search method. Default parameters were used, except for energy evaluations (5×10^5) and docking runs (100). The obtained ligand-DNA complex structure with the lowest docking energy was then subjected to energy minimization in SYBYL. The minimization was first performed as described above, and then the resulting structure was solvated with a monolayer of water molecules for further computation. The solvated system was minimized by fixing the DNA and ligand molecules, followed by relaxing the entire system. The two-step solvation calculations were carried out by using an energy-gradient-convergence criterion of 0.05 kcal/(mol·Å) and a dielectric constant of 1.

For modeling on minor groove binding, the X-ray crystal structure of DNA dodecamer $d(CGCAAATTTGCG)_2$ complexed with Hoechst 33258 (PDB code 264D) was used to prepare the target site for docking calculations. The ligand and water molecules were removed, and then polar hydrogens and Kollman United-Atom charges were added to the DNA. This DNA structure was used for the docking study in the minor groove region. A grid box was set to enclose the binding site of Hoechst 33258 with dimensions of 22.5 × 22.5 × 22.5 Å and a grid spacing of 0.375 Å. Docking was performed by using the same algorithms and parameters as mentioned above. The best-scoring docked model was energy minimized by employing the Powell method with an energy-gradient-convergence criterion of 0.1 kcal/(mol·Å) and a distance-dependent dielectric constant of 4r. The resulting structure was then solvated with a monolayer of water molecules, and the energy was minimized by relaxing the entire system by using an energy-gradient-convergence criterion of 0.1 kcal/(mol·Å) and a dielectric constant of 1. In the present study, computer simulations were performed on Octane and Origin 3800 Silicon Graphics workstations.

DNA Relaxation with Topoisomerase II

Topo II reactions were performed in the reaction buffer (50 mM Tris-HCl [pH 8.0], 120 mM KCl, 10 mM $MgCl_2$, 0.5 mM ATP, 0.5 mM dithiothreitol, 30 mM bovine serum albumin). Plasmid DNA pC86 (1 μg) was incubated with various concentrations of **1**, and was then treated with 8 U topoisomerase II for 30 min at 37ºC. The reaction was stopped by the addition of stop solution (77 mM EDTA, 0.77% SDS) and 1/6 volume 6× loading buffer [43]. The samples were electrophoresed through 1% agarose gel at 60 V for 12 hr in 0.5× Tris-borate-EDTA buffer at room temperature. Next, the gels were stained with ethidium bromide, destained, and then photographed under UV illumination.

Supplemental Data

Supplemental Data include three figures and can be found at http://www.chembiol.com/cgi/content/full/12/12/1317/DC1/.

Acknowledgments

This study was supported by grant NSC90-2320-B-010-074 from the National Science Council, Republic of China. We thank Drs. Terry Beerman, Mary McHugh, Ed Novak, and Ming-Shi Shiao for the advice and comments on the manuscript. L.C.T. also thanks James White for editorial assistance.

Received: May 18, 2005
Revised: September 19, 2005
Accepted: September 26, 2005
Published: December 16, 2005

References

1. Checchi, P.M., Nettles, J.H., Zhou, J., Snyder, J.P., and Joshi, H.C. (2003). Microtubule-interacting drugs for cancer treatment. Trends Pharmacol. Sci. *24*, 361–365.
2. Morrison, C., and Rieder, C.L. (2004). Chromosome damage and progression into and through mitosis in vertebrates. DNA Repair (Amst.) *3*, 1133–1139.
3. Jordan, M.A. (2002). Mechanism of action of antitumor drugs that interact with microtubules and tubulin. Curr. Med. Chem. Anti-Canc. Agents *2*, 1–17.
4. Pratt, W.B., Ruddon, R.W., Ensminger, W.D., and Maybaum, J. (1994). Anticancer Drugs (Oxford, UK: Oxford University Press).
5. Rieder, C.L., and Maiato, H. (2004). Stuck in division or passing through: what happens when cells cannot satisfy the spindle assembly checkpoint. Dev. Cell *7*, 637–651.
6. Johnson, P.A., Clements, P., Hudson, K., and Caldecott, K.W. (1999). A mitotic spindle requirement for DNA damage-induced apoptosis in Chinese hamster ovary cells. Cancer Res. *59*, 2696–2700.
7. Sato, N., Mizumoto, K., Nakamura, M., and Tanaka, M. (2000). Radiation-induced centrosome overduplication and multiple mitotic spindles in human tumor cells. Exp. Cell Res. *255*, 321–326.
8. Neidle, S. (1994). DNA Structure and Recognition (Oxford, UK: Oxford University Press).
9. Snyder, R.D., Ewing, D.E., and Hendry, L.B. (2004). Evaluation of DNA intercalation potential of pharmaceuticals and other chemicals by cell-based and three-dimensional computational approaches. Environ. Mol. Mutagen. *44*, 163–173.
10. Utsuno, K., Maeda, Y., and Tsuboi, M. (1999). How and how much can Hoechst 33258 cause unwinding in a DNA duplex? Chem. Pharm. Bull. (Tokyo) *47*, 1363–1368.
11. Utsuno, K., Kojima, K., Maeda, Y., and Tsuboi, M. (1998). The average unwinding angle of DNA duplex produced by the binding of chromomycin A3. Chem. Pharm. Bull. (Tokyo) *46*, 1667–1671.
12. Bates, A.D., and Maxwell, A. (1993). DNA Topology (Oxford, UK: Oxford University Press).
13. Kim, Y., Geiger, J.H., Hahn, S., and Sigler, P.B. (1993). Crystal structure of a yeast TBP/TATA-box complex. Nature *365*, 512–520.
14. Kim, J.L., Nikolov, D.B., and Burley, S.K. (1993). Co-crystal structure of TBP recognizing the minor groove of a TATA element. Nature *365*, 520–527.
15. Ferguson, L.R., and Denny, W.A. (1979). Potential antitumor agents. 30. Mutagenic activity of some 9-anilinoacridines: relationships between structure, mutagenic potential, and antileukemic activity. J. Med. Chem. *22*, 251–255.
16. Strekowski, L., Mokrosz, J.L., Wilson, W.D., Mokrosz, M.J., and Strekowski, A. (1992). Stereoelectronic factors in the interaction with DNA of small aromatic molecules substituted with a short cationic chain: importance of the polarity of the aromatic system of the molecule. Biochemistry *31*, 10802–10808.
17. Shen, Y.C., Chen, C.Y., Hsieh, P.W., Duh, C.Y., Lin, Y.M., and Ko, C.L. (2005). The preparation and evaluation of 1-substituted 1,2,3,4-tetrahydro- and 3,4-dihydro-beta-carboline derivatives as potential antitumor agents. Chem. Pharm. Bull. (Tokyo) *53*, 32–36.
18. Tu, L.C., Chou, C.K., Chen, C.Y., Chang, Y.T., Shen, Y.C., and Yeh, S.F. (2004). Characterization of the cytotoxic mechanism of Mana-Hox, an analog of manzamine alkaloids. Biochim. Biophys. Acta *1672*, 148–156.
19. Munson, P.J., and Rodbard, D. (1980). Ligand: a versatile computerized approach for characterization of ligand-binding systems. Anal. Biochem. *107*, 220–239.
20. Dassonneville, L., Bonjean, K., De Pauw-Gillet, M.C., Colson, P., Houssier, C., Quetin-Leclercq, J., Angenot, L., and Bailly, C. (1999). Stimulation of topoisomerase II-mediated DNA cleavage by three DNA-intercalating plant alkaloids: cryptolepine, matadine, and serpentine. Biochemistry *38*, 7719–7726.
21. Bonjean, K., De Pauw-Gillet, M.C., Defresne, M.P., Colson, P., Houssier, C., Dassonneville, L., Bailly, C., Greimers, R., Wright,

C., Quetin-Leclercq, J., et al. (1998). The DNA intercalating alkaloid cryptolepine interferes with topoisomerase II and inhibits primarily DNA synthesis in B16 melanoma cells. Biochemistry *37*, 5136–5146.

22. Goodsell, D.S., Morris, G.M., and Olson, A.J. (1996). Automated docking of flexible ligands: applications of AutoDock. J. Mol. Recognit. *9*, 1–5.
23. Morris, G.M., Goodsell, D.S., Huey, R., and Olson, A.J. (1996). Distributed automated docking of flexible ligands to proteins: parallel applications of AutoDock 2.4. J. Comput. Aided Mol. Des. *10*, 293–304.
24. Chen, A.Y., Yu, C., Bodley, A., Peng, L.F., and Liu, L.F. (1993). A new mammalian DNA topoisomerase I poison Hoechst 33342: cytotoxicity and drug resistance in human cell cultures. Cancer Res. *53*, 1332–1337.
25. Chen, A.Y., Yu, C., Gatto, B., and Liu, L.F. (1993). DNA minor groove-binding ligands: a different class of mammalian DNA topoisomerase I inhibitors. Proc. Natl. Acad. Sci. USA *90*, 8131–8135.
26. Laiho, M., and Latonen, L. (2003). Cell cycle control, DNA damage checkpoints and cancer. Ann. Med. *35*, 391–397.
27. Su, T.T., and Vidwans, S.J. (2000). DNA defects target the centrosome. Nat. Cell Biol. *2*, E28–E29.
28. Jenkins, T.C. (1997). Drug-DNA Interaction Protocols (Totowa, NJ: Human Press).
29. Baruah, H., Rector, C.L., Monnier, S.M., and Bierbach, U. (2002). Mechanism of action of non-cisplatin type DNA-targeted platinum anticancer agents: DNA interactions of novel acridinylthioureas and their platinum conjugates. Biochem. Pharmacol. *64*, 191–200.
30. Hayashi, K., Nagao, M., and Sugimura, T. (1977). Interactions of norharman and harman with DNA. Nucleic Acids Res. *4*, 3679–3685.
31. Wilson, W.D., Barton, H.J., Tanious, F.A., Fong, S.B., and Strekowski, L. (1990). The interaction with DNA of unfused aromatic systems containing terminal piperazino substituents. Biophys. Chem. *35*, 227–243.
32. Wilson, W.D. (1990). Nucleic Acids in Chemistry and Biology, Volume Eight, Chapter 8 (Oxford, UK: IRL Press).
33. Stuhlmeier, K.M. (2000). Effects of quinacrine on endothelial cell morphology and transcription factor-DNA interactions. Biochim. Biophys. Acta *1524*, 57–65.
34. Funayama, Y., Nishio, K., Wakabayashi, K., Nagao, M., Shimoi, K., Ohira, T., Hasegawa, S., and Saijo, N. (1996). Effects of β- and γ-carboline derivatives of DNA topoisomerase activities. Mutat. Res. *349*, 183–191.
35. Fesen, M., and Pommier, Y. (1989). Mammalian topoisomerase II activity is modulated by the DNA minor groove binder distamycin in simian virus 40 DNA. J. Biol. Chem. *264*, 11354–11359.
36. Holm, C. (1994). Coming undone: how to untangle a chromosome. Cell *77*, 955–957.
37. Skoufias, D.A., Lacroix, F.B., Andreassen, P.R., Wilson, L., and Margolis, R.L. (2004). Inhibition of DNA decatenation, but not DNA damage, arrests cells at metaphase. Mol. Cell *15*, 977–990.
38. Bailly, C., Dassonneville, L., Colson, P., Houssier, C., Fukasawa, K., Nishimura, S., and Yoshinari, T. (1999). Intercalation into DNA is not required for inhibition of topoisomerase I by indolocarbazole antitumor agents. Cancer Res. *59*, 2853–2860.
39. Baguley, B.C., Denny, W.A., Atwell, G.J., and Cain, B.F. (1981). Potential antitumor agents. 34. Quantitative relationships between DNA binding and molecular structure for 9-anilinoacridines substituted in the anilino ring. J. Med. Chem. *24*, 170–177.
40. Matsuba, Y., Edatsugi, H., Mita, I., Matsunaga, A., and Nakanishi, O. (2000). A novel synthetic DNA minor groove binder, MS-247: antitumor activity and cytotoxic mechanism. Cancer Chemother. Pharmacol. *46*, 1–9.
41. Chevray, P.M., and Nathans, D. (1992). Protein interaction cloning in yeast: identification of mammalian proteins that react with the leucine zipper of Jun. Proc. Natl. Acad. Sci. USA *89*, 5789–5793.
42. Grem, J.L., Politi, P.M., Berg, S.L., Benchekroun, N.M., Patel, M., Balis, F.M., Sinha, B.K., Dahut, W., and Allegra, C.J. (1996). Cytotoxicity and DNA damage associated with pyrazoloacridine in MCF-7 breast cancer cells. Biochem. Pharmacol. *51*, 1649–1659.
43. Yamashita, Y., Kawada, S., Fujii, N., and Nakano, H. (1991). Induction of mammalian DNA topoisomerase I and II mediated DNA cleavage by saintopin, a new antitumor agent from fungus. Biochemistry *30*, 5838–5845.